DOI: 10.1021/ma100428a

Macromolecules
ARTICLE

Solution Behavior of Polystyrene−Polyisoprene Miktoarm Block Copolymers in a Selective Solvent for Polyisoprene

Juan Pablo Hinestrosa,[†] Jose Alonzo,[†] Masashi Osa,[‡] and S. Michael Kilbey II*[,§,⊥]

[†]*Department of Chemical and Biomolecular Engineering, Clemson University, Clemson, South Carolina 29634,* [‡]*Department of Polymer Chemistry, Kyoto University, Katsura, Kyoto, 615-8510, Japan,* [§]*Department of Chemistry, University of Tennessee, Knoxville, Tennessee 37996, and* [⊥]*Center for Nanophase Materials Sciences, Oak Ridge National Laboratory, Oak Ridge, Tennessee 37831*

Received February 23, 2010; Revised Manuscript Received June 28, 2010

ABSTRACT: The dynamics and self-assembly of polystyrene− (PS−) polyisoprene (PI) miktoarm (mixed-arm) block copolymers in *n*-hexane, a selective solvent for PI, are investigated. The miktoarms present a branched arrangement in the soluble block in the fashion of PI−$(PI)_2$, where two PI blocks are connected by a common end point to a linear PS−PI diblock. It is found that these copolymers self-assemble into spherical micelles having cores composed of the insoluble PS blocks and coronas of the well-solvated PI−$(PI)_2$ blocks. Micelles formed from the branched polymer amphiphiles are more compact, having smaller sizes than the micelles formed from a linear PS−PI diblock copolymer of similar molecular weight and composition. As the concentration is decreased, the micelles with large aggregation numbers remain stable, only showing changes in the aggregation number. The hydrodynamic sizes and aggregation numbers determined from the micelles formed from miktoarm copolymers differ from theoretical predictions for spherical micelles made of the equivalent linear amphiphilic diblock copolymers. These differences may arise from the arrangements of the branched blocks inside the micellar corona.

Introduction

Amphiphilic block copolymers are widely studied due to their ability to form organized aggregates in solution and various microphase segregated morphologies in bulk, and because their surfactant-like nature promotes self-assembly onto solid substrates. The morphologies of the aggregates in solution depend on the chemical nature of the blocks, their size and connectivity (chain architecture), temperature, and solvent conditions.[1,2] Applications for those self-organized structures include the generation of templates for inorganic membrane synthesis, separation agents for removal of contaminants water and delivery of therapeutics.[1] These and other applications as well as preparation techniques for block copolymer aggregates have been reviewed recently by Gohy[3] and Riess.[4]

In addition to technological applications, interest in the self-organization of amphiphilic block copolymers springs from conceptual ties to biology: Self-assembly is used by nature to create useful and functional structures such as lipid and cell membranes and virus particles.[1] Because of the intrinsic characteristics of block copolymers, they serve as simple models for more complex systems; consequently, by studying their behavior, it is possible to comprehend how sequence, topology, and composition impact self-assembly, structure, and dynamics in soft matter. As pointed out by Ge and Liu in their recent review article,[5] advances in polymer syntheses have enabled "bio-inspired" amphiphilic and doubly hydrophilic block copolymers of various macromolecular topologies to be readily made, stimulating efforts to understand the links between polymer architecture and supramolecular assembly of those nonlinear amphiphilic block copolymers in aqueous solutions. Of course, copolymers based on polystyrene (PS) and polyisoprene (PI) constituents remain widely studied because these monomers are perhaps the best behaved in living anionic polymerization, providing control over key molecular variables such as composition, block size, and polydispersity and enabling well-defined complex, nonlinear architectures to be synthesized. In particular, the solution behavior of micellized linear PS−PI block copolymers in a selective solvent for PI has been thoroughly studied in relation to the effects of block size, solvent quality, and temperature.[6−13] In this work, we focus on the self-assembly and aggregation properties of micelles made from architecturally complex block copolymers having PS and PI blocks (see Figure 1), which in comparison have been studied to a much more limited extent.

Lazzaroni and co-workers investigated the effect of cyclization by comparing the solution structure of linear and cyclized PS−PI copolymers of the same molar mass and composition in *n*-heptane, a selective solvent for PI.[14] They found that the linear copolymer self-organizes into a "classical" spherical morphology with the PS blocks trapped inside the core of the micelle and the corona formed by the PI chains. However, the cyclic version of the copolymer self-assembles into a sunflower configuration at low concentrations (∼0.01 mg/mL), while at intermediate and high concentrations (∼1 mg/mL), these sunflowers tend to undergo supramolecular assembly and create large wormlike micelles. Borsali et al. studied the solution behavior of graft copolymers consisting of poly(chloroethyl vinyl ether) backbones with grafted PS−PI side chains with similar degrees of polymerization of both the PS and the PI blocks.[15] Selective solvents for PI, *n*-heptane and *n*-decane, were used and it was found that these comb-like structures exist as isolated unimers in the concentration range 0.5−5 mg/mL.[15] The complex architecture prevents any type of aggregation mainly due to the large entropic penalty incurred by bringing the insoluble blocks together. They also found that if the PI block was smaller than the PS block, the graft copolymer was insoluble in solvents that are selective for PI.[15]

Pispas and co-workers have worked extensively with star copolymers made by connecting PS and PI chains to a central core.[16,17]

*Corresponding author.

 Published on Web 08/12/2010

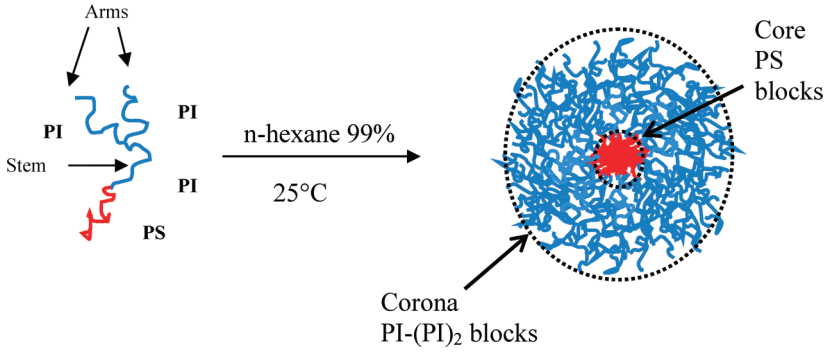

Figure 1. Illustration of a single PS−PI−$(PI)_2$ miktoarm block copolymer and their self-assembly into spherical micelles.

Table 1. Properties of PS−PI and PS−PI−$(PI)_2$ Miktoarm Block Copolymers with Block Molecular Weights given in kDa

sample ID	block M_w's	M_w(PS) (kDa)	M_w(PI) (kDa)	N_{PS}	N_{PI}	PDI	dn/dc^b
DB[a]	PS−PI 26/141	26	141	250	2073	1.09	0.224
MA1	PS−PI−$(PI)_2$ 33/32/$(14)_2$	33	60	317	882	1.01	0.219
MA3	PS−PI−$(PI)_2$ 29.6/70/$(43)_2$	29.6	156	284	2294	1.17	0.207
MA4	PS−PI−$(PI)_2$ 33/33/$(57.8)_2$	33	148.6	317	2185	1.14	0.199

[a] Obtained from Polymer Source, Inc. [b] Measured at λ = 658 nm.

They studied the micellization behavior of $(PS)_2$−PI and PS−$(PI)_2$ block copolymers in *n*-decane, comparing the micelle properties of those 3-arm stars to those formed from linear PS−PI block copolymers.[16] The copolymers were synthesized by anionic polymerization to produce polymers having the same total molecular weight, $M_{w,tot}$, and PS mass fraction. They found that micelles made from miktoarm star copolymers were smaller in size compared to those formed from the linear analogues. The hydrodynamic radius, R_h, and aggregation number, Q, were found to increase in the order PS−$(PI)_2$ < $(PS)_2$−PI < PS−PI. This trend was attributed to the micelles formed from PS−$(PI)_2$ having the largest area per junction point at the core/corona interface and the micelles formed from PS−PI having the smallest. All of the micellar aggregates had spherical morphologies with the PI blocks adopting a stretched conformation in comparison to their unperturbed size. The same group later studied PS−$(PI)_3$ miktoarm stars in *n*-decane.[17] Static and dynamic light scattering experiments revealed spherical aggregates with narrow hydrodynamic size distributions. They found that keeping the degree of polymerization of the soluble block, N_A, constant while increasing the degree of polymerization of the insoluble block, N_B, tends to increase Q. They also showed that Q increases when N_A is reduced and N_B is kept constant. For the PS−$(PI)_3$ stars, the trends in R_h and Q as N_A and N_B are changed are in agreement with what has been theoretically predicted for spherical micelles made from linear diblock copolymers.[18−20] When the effects of concentration were explored, it was found that at high concentrations (~10 mg/mL) the equilibrium shifts toward monodisperse micelles, but at low concentrations (~0.9 mg/mL) a coexistence between unimers and micelles is observed.[17]

The study of the self-assembly of novel branched block copolymers is of significant interest because branching introduces conformation-induced constraints that impact the relaxation dynamics and self-organization.[21] Additionally, branched chains provide a greater number of end-groups, which allows an enhancement of interfacial chemistry and reactivity.[22,23] Understanding the solution behavior of these novel miktoarm (mixed arm) copolymers also helps to further comprehend the process of preferential adsorption at the solid/fluid interface, which has been published separately.[24] In this work, the solution behavior of model PS−PI−$(PI)_2$ block copolymers is studied using static and dynamic light scattering techniques. The aim is to provide further insight into the effect of architecture and molecular asymmetry on the self-assembly in solution of these precisely designed materials, as well as to compare the results with theoretical predictions for micelles made from equivalent linear block copolymers in dilute solution.[19]

Experimental Section

Materials and Sample Preparation. As outlined in our previous contribution,[24] PS−PI−$(PI)_2$ miktoarm block copolymers were synthesized via anionic polymerization using chlorosilane coupling to graft two PI anions and a PS−PI diblock copolymer at a single junction (see Figure 1). The coupling of living macroanions using chlorosilanes has been reviewed recently.[25] Here trichlorosilane is used to produce a three-arm product. The identification strings used to refer to the various copolymers as well as the M_w of each block and polydispersities are shown in Table 1.

The solvent used in these studies is *n*-hexane, which is selective for PI. The solubility parameters (in $(cal/cm^3)^{1/2}$) are δ_{PS} = 9.1, δ_{PI} = 8.1, and $\delta_{n\text{-hexane}}$ = 7.3.[26] Stock solutions in *n*-hexane were prepared gravimetrically by adding solvent to the bulk polymer in dust-free vials. The *n*-hexane was filtered through Millpore 0.2 μm PTFE filters prior to solution preparation. Stock solutions were equilibrated at room temperature for at least a week. 48 to 72 h prior to a light scattering experiment, an aliquot was taken from the stock solution and diluted with filtered *n*-hexane (0.2 μm PTFE) to achieve the concentration desired. Concentrations of 30 and 3 μg/mL (0.03 and 0.003 mg/mL) were used.

Static and Dynamic Light Scattering. Light scattering measurements were performed on a four detector ALV goniometer equipped with a linearly polarized 22 mW HeNe laser operating at a wavelength, λ, of 632.8 nm. The signal is processed using an ALV 5000 multiple tau digital correlator with an initial sampling time of 125 ns. The temperature is maintained at 25 ± 0.1 °C in all experiments. The copolymer solutions were contained in dust-free 10 mm borosilicate glass cuvettes that were sealed with a Teflon cap and the total volume used was 1.5 mL. All of the samples were filtered using a 0.2 μm PTFE filter immediately before filling the glass cuvettes.

A total of 16 angles ranging from 20° to 146° are used in the dynamic light scattering (DLS) experiments. A counting time of 600 s is used at each angle in order to obtain reliable statistics for the light intensity autocorrelation function, $g_2(q,\tau)$, defined by

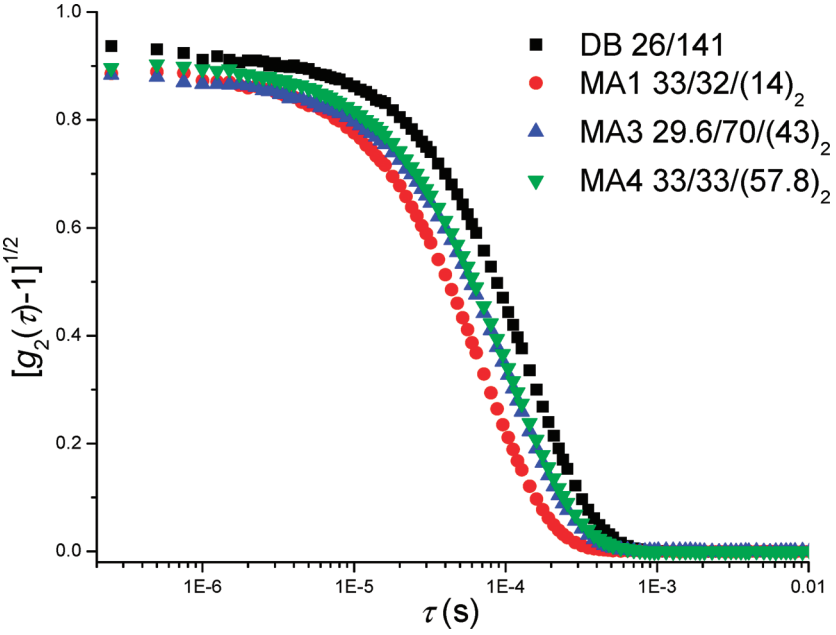

Figure 2. Light intensity autocorrelation function for all samples at 30 μg/mL in *n*-hexane at $\theta = 96°$. The legend shows the sample ID strings and molecular weights (in kDa) of each copolymer studied.

the Siegert relation as[27]

$$g_2(q,\tau) = 1 + g_1(q,\tau)^2 = \frac{\langle I(q,t)I(q,t+\tau)\rangle}{\langle I(q,t)^2\rangle} \quad (1)$$

where $I(q,t)$ is the scattered light intensity at time t and $g_1(q,\tau)$ is the first-order electric field time correlation function, which depends on the delay time τ and the scattering wave vector, q. The latter is experimentally determined from the scattering angle θ, λ and the solvent refractive index, n_D, as $q = (4\pi n_D/\lambda)\sin(\theta/2)$. As an example, the autocorrelation function profiles, expressed as $[g_2(q,\tau) - 1]^{1/2}$ versus τ, are shown in Figure 2 for all of the copolymer solutions studied at 30 μg/mL and $\theta = 96$. The autocorrelation functions determined at each scattering angle were analyzed first by the CONTIN[28] algorithm (built into the ALV software) to determine the distribution of decay rates, $A(\Gamma)$, which provides insight into the population(s) of scatterers in solution. CONTIN uses a regularization method in order to resolve $A(\Gamma)$ such that it satisfies the expression[29]

$$[g_2(\tau) - 1]^{1/2} = g_1(\tau) = \int_0^\infty A(\Gamma)e^{-\Gamma\tau}\,d\Gamma \quad (2)$$

For systems where the CONTIN analysis shows one peak in the distribution of decay rates, the method of cumulants[30] is used to resolve the mean decay rate or first cumulant, Γ_1, and the variance, μ_2/Γ_1^2, at each scattering angle according to:

$$\frac{1}{2}\ln[g_2(\tau) - 1] = \Gamma_0 - \Gamma_1\tau + \frac{\mu_2}{2}\tau^2 \quad (3)$$

Γ_0 is a constant independent of τ. Data and fitting results (up to 90% of the correlation function decay) using the method of cumulants are shown in the Supporting Information (Figure S1) for sample MA1 at 30 μg/mL at four scattering angles. Once the characteristic decay rates are obtained, the apparent diffusion coefficient, D_{app}, from a population having a mean decay rate of Γ_i can be determined by[31]

$$D_{app}(q) \equiv \frac{\Gamma_i}{q^2} \quad (4)$$

The "true" z-average diffusion coefficient, $\langle D\rangle_Z$, is obtained by extrapolating $D_{app}(q)$ to zero scattering angle ($q^2 \to 0$), where nondiffusional processes such as rotation or polymer segment fluctuations do not contribute to $g_1(q,\tau)$.[27] After determining $\langle D\rangle_Z$, the hydrodynamic radius, R_h, is calculated using the Stokes–Einstein equation, $R_h = kT/6\pi\eta_o\langle D\rangle_Z$, where k is the Boltzmann constant, T is the absolute temperature and η_o is the solvent viscosity ($\eta_o = 0.293$ cP for *n*-hexane at 25 °C).[27]

Static light scattering (SLS) experiments were also carried out using the ALV system. A total of 44 scattering angles ranging from 20° to 152° were surveyed and toluene was used as the calibration standard. The apparent molecular weight, $M_{w,app}$, and *z*-average radius of gyration, $R_g \equiv [\langle S^2\rangle_z]^{1/2}$, were determined using the truncated form of the virial expansion for the scattered intensity:[27]

$$\frac{Kc}{\Delta R} = \frac{1}{M_{w,app}P(q)} + 2A_2c \quad (5)$$

Here c is the solution concentration, ΔR is the normalized absolute scattering intensity, A_2 is the second virial coefficient and $P(q)$ is the so-called particle form factor. K is the contrast factor, which is defined as:[27]

$$K = \frac{16\pi^2}{\lambda^4 N_{av}} n_D{}^2 \left(\frac{dn}{dc}\right)^2 \quad (6)$$

where N_{av} is Avogadro's number and dn/dc is the refractive index increment, which was measured using a Wyatt OptiLab Rex differential refractometer at $\lambda = 658$ nm. Results from those dn/dc measurements are shown in Table 1. Because of the low concentrations studied and the low values of A_2 typically observed ($\sim 10^{-5}$ cm^3 mol/g^2),[16,17] the second term of eq 5 can be neglected. For comparatively small particles ($q^2R_g{}^2 \ll 1$), $P(q)$ can be expressed as:[27]

$$P(q) = 1 + \frac{q^2R_g{}^2}{3} \quad (7)$$

The aggregation number, Q, is obtained by comparing the $M_{w,app}$ determined by SLS with the molecular weight of the single block copolymer chains: $Q = M_{w,app}/M_{w,tot}$ where $M_{w,tot} = M_{w,PS} + M_{w,PI}$ ($M_{w,PS}$ and $M_{w,PI}$ values are listed in Table 1). This parameter provides an estimate of the number of single chains self-assembled into the micellar aggregate.

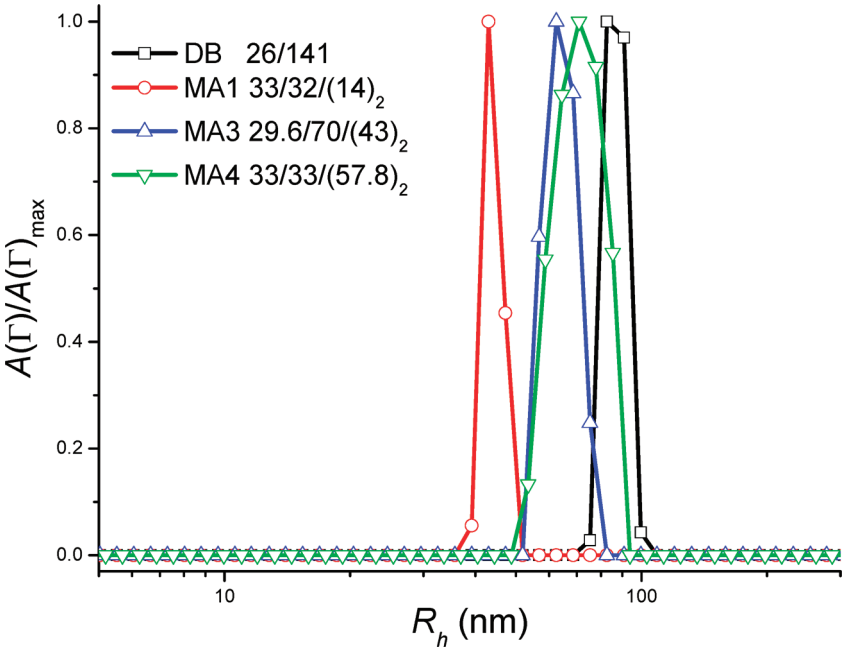

Figure 3. Hydrodynamic radii, R_h, distributions obtained from CONTIN regularization method for PS−PI−$(PI)_2$ miktoarm and PS−PI linear block copolymers at $c = 30\ \mu g/mL$ and $\theta = 96°$. One narrow size distribution is observed for each sample, which is commonly found for micellized block copolymers.

Results and Discussion

Hydrodynamic size distributions obtained for samples at 30 μg/mL from the CONTIN regularization method (see Figure 3) show narrow monodisperse behavior, which is characteristic of well-defined micellar aggregates of block copolymers,[32] and the normalized amplitude $A(\Gamma)/A(\Gamma)_{max}$ allows direct comparison of their R_h distributions. The fact that the R_h values range from 40 nm for sample MA1 to 90 nm for sample DB provides an indication that these block copolymers are in an aggregated state, as these sizes are too large for single PS−PI−$(PI)_2$ chains in solution (see analysis in the Appendix). The hydrodynamic size distributions obtained by DLS suggest that these copolymers self-assemble in solution, most likely to due to the low solubility of the PS blocks in *n*-hexane. Because the R_h distributions determined at each scattering angle for all of the samples at 30 μg/mL show only one narrow distribution peak, the method of cumulants (eq 3) can be used to determine the mean decay rate Γ_1 from the $[g_2(\tau) - 1]^{1/2}$ profiles. The resulting Γ_1 as a function of q^2 are shown in the Supporting Information (Figure S2). There it is observed that all of the systems studied at 30 μg/mL display a linear dependence on q^2 and intersect the *y*-axis at $\Gamma_1 \approx 0$. This behavior is expected for particles solely controlled by diffusive processes; thus, the diffusion coefficient can be obtained from the slope of the line.[27] Further information from the DLS results can be obtained by plotting D_{app} versus q^2, which is shown in Figure 4. It is observed that D_{app} has no *q*-dependence over the range studied, and a linear fit and extrapolation to $q^2 \rightarrow 0$ provides $\langle D \rangle_Z$. This *q* independency is an indication of hard-sphere diffusive behavior.[33] The R_h for each sample can be calculated from $\langle D \rangle_Z$ using the Stokes−Einstein equation and the values of $\langle D \rangle_Z$ and R_h obtained are reported in Table 2. It is worth noting that the $\langle D \rangle_Z$ found by extrapolation to $q^2 \rightarrow 0$ are within 3% of the diffusion coefficients obtained from a linear fit of the results shown in Figure S2 (with the fit forced through $\Gamma_1 = 0$).

It is seen clearly from Figure 4 that the aggregates formed from sample MA1, the smallest (lowest $M_{w,tot}$) branched copolymer, diffuse at a faster rate than the aggregates formed by the larger branched copolymers MA3 and MA4 and the linear DB sample. Samples MA3 and MA4 have very similar dynamic behavior despite having different sized "arms" and "stems", as seen from Table 1. Their linear analogue, sample DB, which has an $M_{w,tot}$ and composition similar to MA3 and MA4, has a much slower diffusion rate, implying a larger hydrodynamic size. This pattern of behavior was also observed in the near-surface (effective) diffusion coefficients determined from studies of the kinetics of adsorption of these macromolecular ensembles at the solid/fluid interface.[24] As expected, micelles formed from sample DB have the smallest $\langle D \rangle_Z$ (largest R_h) while samples MA3 and MA4 have similar R_h values of ≈64 nm. It is interesting to compare samples MA3 and MA4 with sample DB, since their $M_{w,tot}$ and N_{PS} and N_{PI} values are rather similar. Branching in the PI blocks of MA3 and MA4 makes the micelles more compact in terms of size compared to those formed from the linear analogue, sample DB. This behavior is in agreement with the findings of Pispas and coworkers, where the micelles formed from PS−$(PI)_2$[16] and PS−$(PI)_3$[17] miktoarm block copolymers in *n*-decane were compared to the micelles formed from linear PS−PI copolymers of similar composition and $M_{w,tot}$.

Figure 5 shows the SLS results for the PS−PI and PS−PI−$(PI)_2$ samples at 30 μg/mL. The near-linear relationship of $(Kc/\Delta R)^{1/2}$ over the *q*-range studied allows $M_{w,app}$ and R_g to be easily determined using eq 5, and those values are presented in Table 2. The R_g/R_h ratio offers an indication of the aggregate morphology and as reported in Table 2, all of the values are around 0.7, which is expected for spherical aggregates.[33] This result along with the behavior shown in Figure 4 confirm that these novel miktoarm block copolymers self-assemble into spherical "star-like" micelles, having cores that consist of the insoluble PS blocks and coronas made of the well-solvated PI−$(PI)_2$ blocks, as illustrated in Figure 1. Similar to what was observed from the R_h values, the linear DB sample has a larger R_g compared to samples MA3 and MA4 and sample MA1 has the smallest R_g. Aggregation numbers, *Q*, for all of the copolymers studied are shown in Table 2.

The results presented here also show that samples MA1 and MA4 have very similar *Q* values despite differences in the sizes of their soluble PI blocks. This shows the strong influence of the degree of polymerization of insoluble PS block, N_{PS}, on the self-assembly of block copolymers. In particular, samples MA1 and MA4 both feature PS blocks and PI stems of similar M_w; thus,

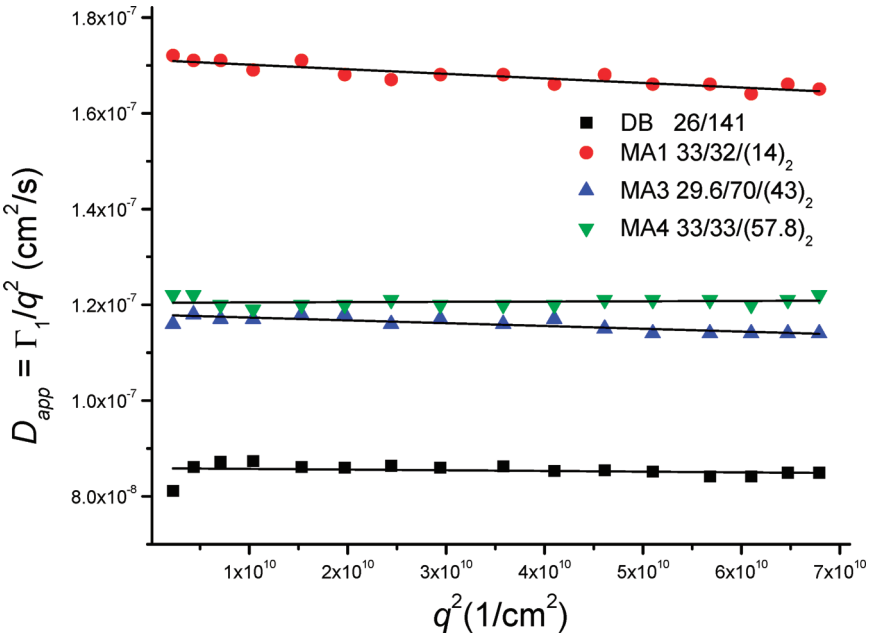

Figure 4. Apparent diffusion coefficient D_{app} versus q^2 for micellized PS−PI−$(PI)_2$ miktoarm and PS−PI linear block copolymers at $c = 30\ \mu$g/mL in *n*-hexane. Linear fits are shown as solid black lines. The independence of D_{app} with respect to q^2 suggests hard-sphere diffusive behavior.

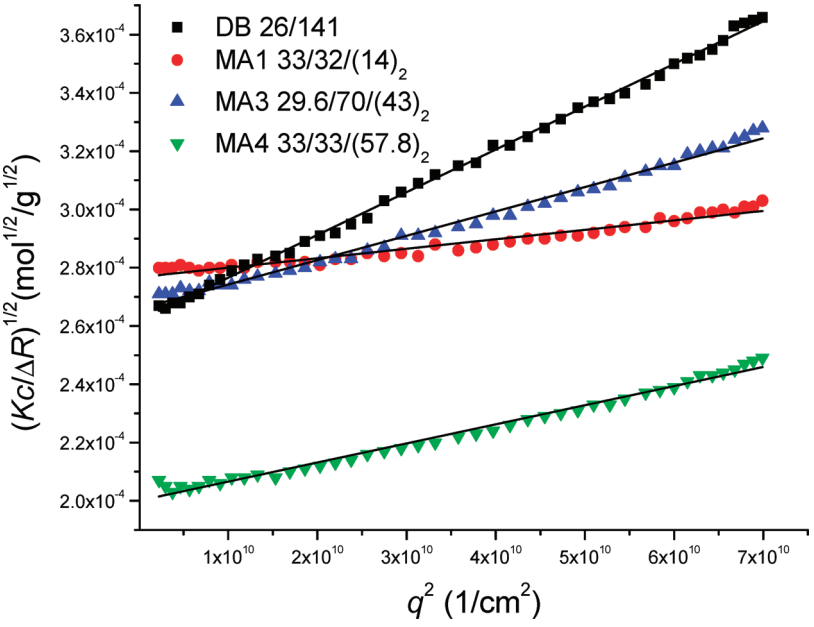

Figure 5. Berry plot from SLS experiments for all samples studied at $c = 30\ \mu$g/mL. The linear behavior over the *q*-range studied allows eq 5 to be used to properly fit the data (solid black lines).

Table 2. Solution Properties at $c = 30\ \mu$g/mL for PS−PI and PS−PI−$(PI)_2$ Miktoarm Block Copolymers in *n*-Hexane

sample ID	and block M_w's	$\langle D\rangle_Z$ (cm^2/s)	R_h (nm)	R_g (nm)	$M_{w,app}$ (kDa)	R_g/R_h	Q
DB	PS−PI 26/141	8.66×10^{-8}	86.0	67.1	1.43×10^4	0.78	85
MA1	PS−PI−$(PI)_2$ 33/32/$(14)_2$	1.71×10^{-7}	43.6	26.6	1.31×10^4	0.61	140
MA3	PS−PI−$(PI)_2$ 29.6/70/$(43)_2$	1.18×10^{-7}	63.2	46.2	1.43×10^4	0.73	77
MA4	PS−PI−$(PI)_2$ 33/33/$(57.8)_2$	1.15×10^{-8}	64.8	47.2	2.52×10^4	0.73	139

their size difference must spring from the degree of polymerization and arrangement of the well-solvated outer $(PI)_2$ blocks, which are likely to adopt a stretched conformation toward the outer edge of the corona. On the other hand, while MA3 and MA4 have similar $M_{w,tot}$ and R_h, their aggregation properties are rather different: for sample MA3 $Q = 77$, while for sample MA4 $Q = 139$. Although the large difference in aggregation number seems surprising at first, it has been theoretically predicted[18] and later experimentally confirmed[19] that $Q \sim N_B^{4/5}$, where N_B is the degree of polymerization of the insoluble block. Thus, sample MA4, which has a larger PS block, has the tendency to incorporate more chains into the macromolecular ensemble than MA3.

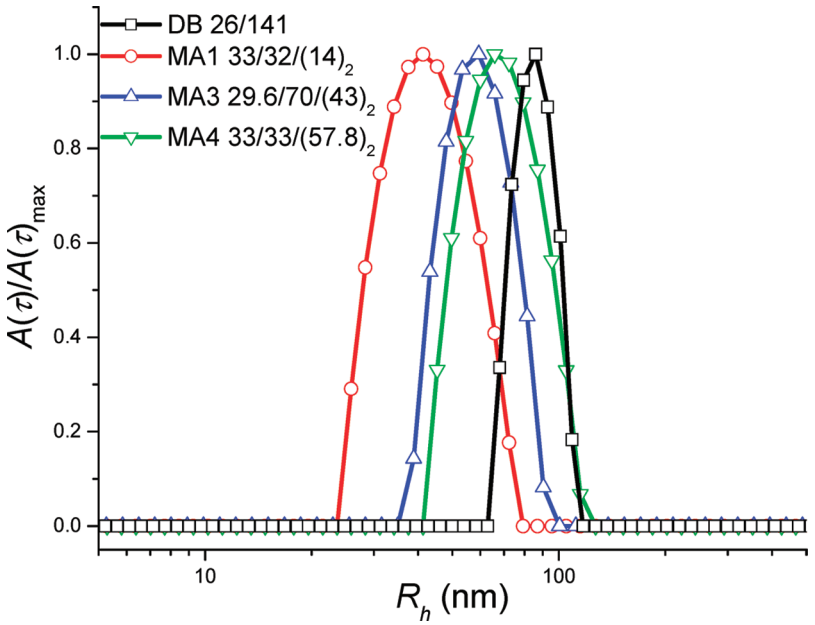

Figure 6. Hydrodynamic radii, R_h, distributions for PS−PI and PS−PI−$(PI)_2$ miktoarm block copolymers at $c = 3\ \mu$g/mL in *n*-hexane, $\theta = 78°$. The same *x*-axis scale is used in Figures 3 and 6.

The influence of the relative sizes of the stem and arms on the arrangement of the branched PI chains of the micellar corona cannot be resolved at this point. Denser packing of chains at the core/corona interface may promote stretching of both PI arms outward from the micelle, similar to the outer region of a multiarm polymer star.[13,34,35] Less compact arrangements may allow one of the arms to configure itself such that it points back toward the core/corona interface—an arrangement revealed through a mean-field treatment of branched polymer brushes that is owed to the branched brush being able to maximize its conformational entropy at a cost of stretching the tethered stem.[36] When taking into account properties of the micelles formed from the linear DB sample, it can be seen that Q is smaller than for MA4 and slightly larger than for MA3. This again shows the strong effect of N_B on the micellar aggregation. However, if N_B was the only parameter determining the number of chains incorporated into the ensemble, Q for sample DB would be lower than Q for MA3 because N_B is smaller for sample DB. As this is found to be not true, it stands to reason that the linear soluble PI blocks of sample DB allow more copolymer chains to self-assemble into the micelle, suggesting that the presence of the branching point in the miktoarms reduces the ability of the branched PI chains to pack, similar to what was found by Pispas et al.[16,17] This behavior likely arises from a larger entropic cost associated with the aggregation of branched copolymers in comparison to linear ones, which may lead to a larger area per chain at the core/corona interface even though the branch point is distal from the interface.

Effects of Dilution. To examine whether the critical micelle concentration, cmc, could be detected for these systems, the solutions at 30 μg/mL were successively diluted by factors of 10 to generate 3, 0.3, and 0.03 μg/mL solutions; however, incoherent scattering became problematic at concentrations below 3 μg/mL. Results from the regularized fitting of the autocorrelation function (using the CONTIN algorithm) measured at $c = 3\ \mu$g/mL are presented in Figure 6. Here it is seen that the distributions of hydrodynamic radii are broader in comparison to the results obtained at 30 μg/mL (The same *x*-axis scale is used in Figures 3 and 6.). The broadness in the hydrodynamic size distribution may be an effect of using the same counting time as for the experiments at 30 μg/mL. The CONTIN regularization method is very sensitive to noise in the correlation function and this noise may lead to a broader size distribution.[37] (A comparison on the effects of counting time in dynamic light scattering experiments is shown in the Supporting Information.) As seen in Figure 6, the linear DB sample retains the narrowest R_h distribution among the samples studied despite having the smallest PS block. All the copolymers studied remain in a micellized state as indicated by the large R_h values obtained. The autocorrelation functions at 3 μg/mL concentration were analyzed by the method of cumulants (eq 3) and as shown in Figure 7, D_{app} is independent of q^2 (as it was at 30 μg/mL) suggesting a spherical arrangement and hard-sphere diffusive behavior.

The R_h values obtained for the macromolecular ensembles at 3 μg/mL are slightly smaller than those determined at 30 μg/mL. These results seem to differ from the decrease in D_{app} (increase in R_h) observed by Pispas et al. for PS−$(PI)_2$ block copolymers in *n*-decane as c was decreased.[16] However, the concentration range studied was from 1 μg/mL to 1000 μg/mL, with only two concentrations below 400 μg/mL.[16] Table 3 summarizes $\langle D\rangle_Z$, R_h, R_g, $M_{w,app}$, R_g/R_h, and Q values obtained for the samples studied at 3 μg/mL.

The results of the SLS experiments at $c = 3\ \mu$g/mL are shown in Figure 8, and the fitting results are given in Table 3. The R_g/R_h ratios for all of the samples are ~0.7, which along with the $D_{app}(q)$ behavior suggests that the micelles remain in a spherical star-like morphology at this ultra low concentration. The Q values determined for the spherically micellized samples MA1, MA3, and MA4 at $c = 3\ \mu$g/mL are slightly different than the ones determined at 30 μg/mL. For MA1 $Q = 153$, which is somewhat greater than at 30 μg/mL, suggesting the ability of the ensembles to incorporate more chains as the system is diluted. An increase in aggregation number upon dilution is also observed for the micelles formed from copolymer MA3: Q changes from 77 to 137; on the other hand, copolymer MA4 shows an opposite trend, with Q decreasing from 137 to 101 upon dilution. The differences in solution behavior of the micelles formed from MA3 and MA4 at $c = 3\ \mu$g/mL are also reflected in their preferential adsorption at the solid/fluid interface: At lower

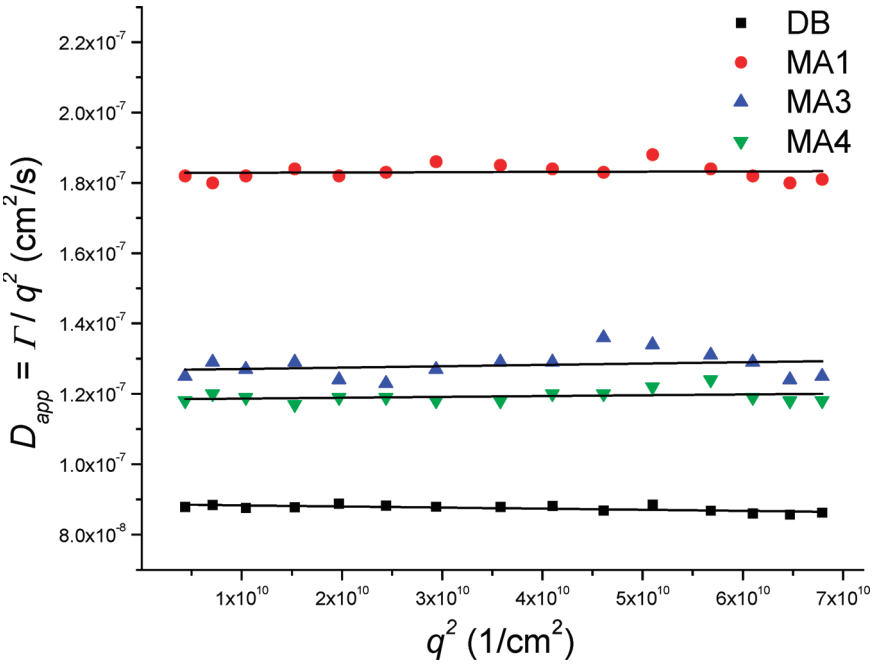

Figure 7. Apparent diffusion coefficient D_{app} versus q^2 for all samples studied at $c = 3\ \mu$g/mL in *n*-hexane. Linear fits are shown by the solid black lines.

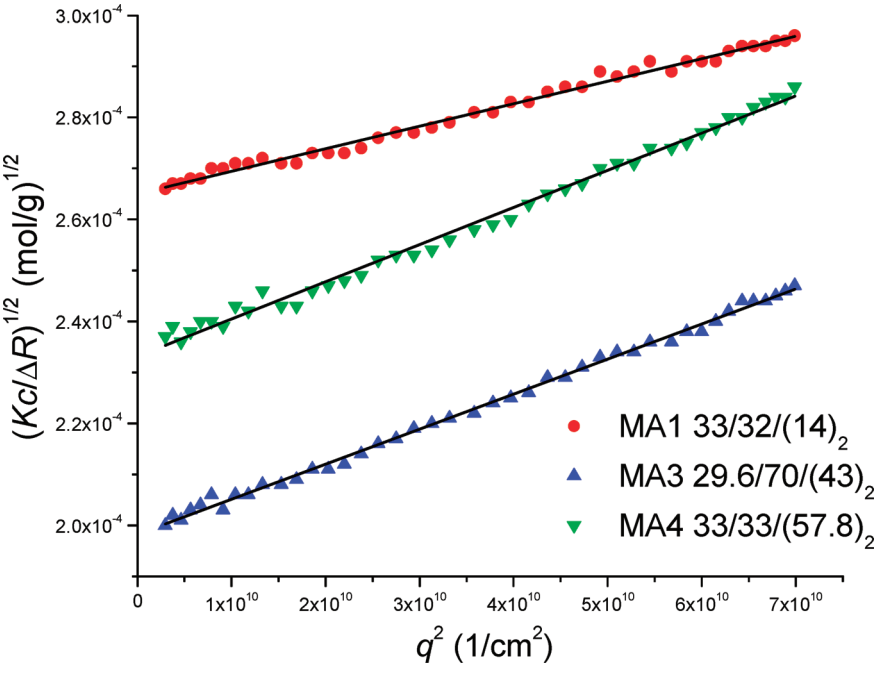

Figure 8. Berry plot for PS−PI−(PI)$_2$ miktoarm block copolymers at $c = 3\ \mu$g/mL in *n*-hexane. Solid black lines are fits obtained using eq 5.

Table 3. Solution Properties at $c = 3\ \mu$g/mL for PS−PI and PS−PI−(PI)$_2$ Miktoarm Block Copolymers in *n*-Hexane

sample ID	$\langle D \rangle_Z$ (cm^2/s)	R_h (nm)	R_g (nm)	$M_{w,app}$ (kDa)	R_g/R_h	Q
DB	8.86×10^{-8}	84.1				
MA1	1.83×10^{-7}	40.8	31.6	1.43×10^4	0.77	153
MA3	1.27×10^{-7}	58.7	45.6	2.54×10^4	0.78	137
MA4	1.18×10^{-8}	62.9	43.3	1.84×10^4	0.69	101

concentration, the preferential adsorption process is dominated by surface relaxation/reorganization events, rather than by transport of micelles in the near-surface region.[24] At this moment, we are uncertain as to why Q changes upon dilution, increasing for MA1 and MA3 but decreasing for MA4, while the R_h values remain nearly constant. When the concentration is reduced and approaches the stability limit for the micelles, i.e., cmc, the driving force for the self-assembly process decreases, impacting both aggregation and size. The micelles may be undergoing a rapid exchange of chains with the bulk solution as described by the closed association model.[32] Additionally, the volume fraction of polymer inside the micellar core, φ, has been shown to have an effect on the equilibrium properties of the macromolecular ensembles.[19,38] Consequently, φ may vary as the solution concentration is decreased. Nevertheless, it is seen that R_h does not show a significant change from 30 to 3 μg/mL; thus, if we conceptualize these spherical micelles as polymer stars

with Q number of arms, a variation in Q should not drastically affect R_h, as has been shown for star homopolymers in good solvents where their size becomes practically independent of the number of arms, f, after $f \geq 8$.[13,33]

Comparison with Predictions for Spherical Diblock Copolymer Micelles. Zhulina and co-workers have developed a comprehensive theoretical framework for examining the dilute solution behavior of diblock copolymer micelles.[19] Their model elucidates and predicts the range of thermodynamic stability and equilibrium properties for spherical, cylindrical, and lamellar morphologies, with experimental verification coming from light scattering and small angle neutron scattering (SANS) experiments on linear PS−PI diblock copolymers in *n*-heptane. As the PS−PI−$(PI)_2$ miktoarm copolymers studied here self-assemble into spherical micelles, the attention is focused on comparisons to predictions for spherical morphologies.

According to Zhulina et al.,[19] the free energy of a spherical block copolymer micelle in solution, F_3, having the insoluble blocks trapped inside the micellar core and the corona arms formed from the solvated blocks can be written as

$$\frac{F_3}{kT} = \frac{3\pi^2 {r_3}^2}{80 p_B N_B} + \gamma \frac{3N_B}{\varphi r_3} + \nu \hat{C}_F {r_3}^{3/2} \left(\frac{\varphi}{3N_B}\right)^{1/2} \ln\left[1 + \frac{1}{\nu}\left(\frac{a_A}{a_B}\right)^{1/\nu} \hat{C}_H N_A {r_3}^{(1-3\nu)/2\nu} \left(\frac{3N_B}{\varphi}\right)^{(\nu-1)/2\nu}\right] \quad (8)$$

In eq 8, the first term corresponds to the free energy of the core blocks (denoted by the subscript B), the second term represents the free energy of the core/corona interface and the third term accounts for the free energy of the solvated corona (denoted by the subscript A). The free energy depends on a variety of parameters: p_A and p_B are the stiffness parameters and a_A and a_B are the monomer sizes for the corona and core constituents, respectively. r_3 is the dimensionless core radius, which is defined as $r_3 = R_3/a_B$, where R_3 is the core radius; φ is the volume fraction of polymer inside the core ($\varphi = 1$ means that the core is in the melt state) and ν is the solvent quality parameter from the well-known relationship between the radius of gyration, R_g, and the degree of polymerization of the soluble block, N_A: $R_g \sim {N_A}^{\nu}$. γ is the surface tension at the core/corona interface, which varies with temperature according to:[19] $\gamma/\varphi^{2/3} = 0.14 - 1.07 \times 10^{-3} T(°C)$. Finally $\hat{C}_F$ and $\hat{C}_H$ are solvent quality dependent numerical prefactors that are expressed in terms of p_A and the excluded volume and three-body interaction parameters, v and ω, respectively:[19]

$$\hat{C}_H = \begin{cases} C_H {p_A}^{1/3} v^{1/3}, & \nu = \frac{3}{5} \\ C_H {p_A}^{1/4} \omega^{1/4}, & \nu = \frac{1}{2} \end{cases}; \qquad \hat{C}_F = \begin{cases} C_F, & \nu = \frac{3}{5} \\ C_F {p_A}^{-3/4} \omega^{1/4}, & \nu = \frac{1}{2} \end{cases} \quad (9)$$

Here C_H and C_F are numerical constants of order unity that were determined from light scattering and SANS experiments on a series of linear PS−PI block copolymers.[19] In the case of good solvent conditions ($\nu = 3/5$), $v = 0.05$ and this can be incorporated into the C_H constant. Under Θ-solvent conditions, ω is incorporated into the values of C_H and C_F.[19]

By minimizing F_3 with respect to r_3 ($\partial F_3/\partial r_3$), a nonlinear equation for r_3 is obtained:

$$\frac{3\pi^2 r_3}{40 p_B N_B} - \gamma \frac{3N_B}{\varphi {r_3}^2} + \frac{3}{2}\nu \hat{C}_F \left(\frac{\varphi}{3N_B}\right)^{1/2} {r_3}^{1/2} \ln\left[1 + \frac{1}{\nu}\left(\frac{a_A}{a_B}\right)^{1/\nu} \hat{C}_H N_A {r_3}^{(1-3\nu)/2\nu} \left(\frac{3N_B}{\varphi}\right)^{(\nu-1)/2\nu}\right] + \frac{\hat{C}_F \hat{C}_H N_A \left(\frac{a_A}{a_B}\right)^{1/\nu} \left(\frac{3N_B}{\varphi}\right)^{-1/2\nu} \left(\frac{1-3\nu}{2\nu}\right) {r_3}^{(1-2\nu)/2\nu}}{1 + \frac{1}{\nu}\left(\frac{a_A}{a_B}\right)^{1/\nu} \hat{C}_H N_A {r_3}^{(1-3\nu)/2\nu} \left(\frac{3N_B}{\varphi}\right)^{(\nu-1)/2\nu}} = 0 \quad (10)$$

Equation 10 can be numerically solved for the dimensionless core radius r_3, This allows R_3 to be calculated, and also the corona thickness, H_3:[19]

$$H_3 = R_3 \left[\left(1 + \frac{1}{\nu}\left(\frac{a_A}{a_B}\right)^{1/\nu} \hat{C}_H N_A {r_3}^{(1-3\nu)/2\nu} \left(\frac{3N_B}{\varphi}\right)^{(\nu-1)/2\nu}\right)^{\nu} - 1\right] \quad (11)$$

Subsequently, the total size of a spherical micelle, ${R_3}^{tot}$, and Q are given by[19]

$$R_3^{tot} = H_3 + R_3 \quad (12)$$

$$Q = \frac{4\pi {r_3}^3 \varphi}{3N_B} \quad (13)$$

However, as stated by Zhulina and co-workers,[19] to compare the experimental R_h values with the ones predicted for spherical micelles, R_h^s, it is necessary to account for the fact that the solvent drains through the macromolecular ensemble on the same scale as the size of the last blob at the periphery of the micelle, ξ_{last}. Thus, the hydrodynamic size of a spherical block copolymer micelle, R_h^s, can be predicted as:

$$R_h^s = R_3^{tot} - C_\xi \xi_{last} = R_3^{tot}\left(1 - \frac{C_\xi}{\sqrt{Q}} {p_A}^{3/4}\right) \quad (14)$$

where C_ξ is a numerical constant of order unity. In our calculations C_ξ is set equal to 1.

To make comparisons between Zhulina's et al. theory and our experimental results, it is necessary to consider that the copolymers studied here have branched coronas with PI−$(PI)_2$ arrangements; therefore, the parameter N_A needs to be modified to account for the smaller size of the branched blocks forming the corona. As shown in the Appendix, calculations of radius of gyration based on chain statistics for the branched PI chains of the PS− PI−$(PI)_2$ miktoarm copolymers in *n*-hexane, $R_{g,br}$, show that the Flory branching parameter, g, is ≈0.8 for three different approaches evaluated. Accordingly, to calculate R_h^s and Q using the framework developed by Zhulina et al.,[19] the N_A values used here were "rescaled" as $N_A = 0.8 N_{PI}$, where N_{PI} are the values given in Table 1. In a sense, this provides insight into whether the equivalent size linear chain forms a micelle with similar properties, namely hydrodynamic size and aggregation number, as the one experimentally found for the corresponding branched miktoarm block copolymer. The parameters and

Table 4. Parameters Used for Predictions of Dilute Solution Spherical Micelles[a]

a_A (Å)	a_B (Å)	p_A	p_B	C_F	C_H
5.0	5.6	1.6	1.5	1.38	0.68

[a] The same parameters were used by Zhulina et al.[19]

Table 5. Solution Properties at $c = 30\ \mu$g/mL in *n*-Hexane and Predictions under Θ Solvent Conditions ($\nu = 0.5$) for PS−PI and PS−PI−$(PI)_2$ Miktoarm Block Copolymers

	experimental results		$\varphi = 0.70$		$\varphi = 0.85$		$\varphi = 1.00$	
sample ID	R_h (nm)	Q	R_h^s (nm)	Q	R_h^s (nm)	Q	R_h^s (nm)	Q
DB	86.0	85	37.2	72	36.6	69	36.2	68
MA1	43.6	140	30.1	155	29.4	150	28.8	145
MA3	63.2	77	37.7	87	37.1	84	36.6	82
MA4	64.8	139	38.8	101	38.2	99	37.7	95

numerical prefactors used in the present calculations are listed in Table 4.

Another important parameter for the prediction is polymer volume fraction inside the core, φ. Often it is assumed that PS−PI micelles have solvent-free PS cores, $\varphi = 1$, because of the high glass transition temperature for PS.[11,16,17] However Zhulina et al.[19] determined that there is some solvent inside the core, and used a value of $\varphi = 0.70$ in their theoretical model. Recently, LaRue et al. used light scattering and X-ray small angle scattering to determine $\varphi = 0.85$ for linear PS−PI diblock copolymers in heptane.[20] In the comparisons done here, it is decided to make the calculations using φ values of 0.70, 0.85, and 1. The solvent quality, through the parameter ν, also plays a role in the equilibrium free energy of spherical micelles. According to Zhulina et al.,[19] in a PS−PI micellar solution in *n*-heptane, the solvent behaves as a Θ solvent. On the other hand, from the determination of R_g for PI homopolymers in *n*-hexane, it is known that $\nu = 0.57$, indicating nearly good solvent conditions (see Appendix); therefore, the comparisons are done for both Θ and good solvent conditions. Tables 5 and 6 show comparisons of the experimental results at $c = 30\ \mu$g/mL and the calculated values for R_h^s and Q.

In both solvent conditions, the theoretical predictions follow the same trend as the experimental findings in this study; i.e., micellar hydrodynamic size increases with $M_{w,tot}$, and Q is highly dependent on and increases with N_B. As anticipated, the Q values decrease as solvent quality increases. When there are no excluded volume interactions among chains, i.e., Θ conditions, the area per chain at the core/corona interface is smaller, which allows more chains to pack into the micellar ensemble. The increased crowding in the micellar corona makes R_h^s values larger compared to those calculated for good solvent conditions. However, the calculated R_h^s differ from the measured R_h for each of the samples studied while the Q values are somewhat close to the ones obtained from SLS experiments. The differences seen in hydrodynamic radii might arise from the organization of the branched blocks, due to additional stretching of the stem in the corona blocks that is not conceived in the model and/or from using the numerical prefactors, C_H and C_F, resulting from fits of experimental results of micelles formed from linear block copolymers, although it should be noted that these parameters are not architecturally dependent. As expected, the largest R_h^s values are achieved using $\varphi = 0.70$ due to the presence of solvent inside the micellar core; however, neither R_h^s nor Q change significantly as φ increases. Despite the correction in N_A introduced to account for branching (see Appendix), the calculated R_h^s values for MA3 and MA4 are slightly larger that the one predicted for sample DB at both solvent conditions. This

Table 6. Solution Properties at $c = 30\ \mu$g/mL in *n*-Hexane and Predictions under Good Solvent Conditions ($\nu = 0.57$) for PS−PI and PS−PI−$(PI)_2$ Miktoarm Block Copolymers

	experimental results		$\varphi = 0.70$		$\varphi = 0.85$		$\varphi = 1.00$	
sample ID	R_h (nm)	Q	R_h^s (nm)	Q	R_h^s (nm)	Q	R_h^s (nm)	Q
DB	86.0	85	31.8	55	31.2	53	30.8	51
MA1	43.6	140	25.9	141	25.1	135	24.5	129
MA3	63.2	77	32.2	68	31.5	67	31.0	65
MA4	64.8	139	33.2	80	32.5	77	31.9	74

behavior differs considerably from our experimental results in which micelles formed from the linear PS−PI block copolymer have much larger R_h, as expected, since branched chains are more compact than their linear analogues.

Regarding the aggregation number, the largest Q values predicted are those for sample MA1, which has a larger N_B and the smallest ratio of PI to PS in comparison to samples MA3 and MA4. These observed behaviors reflect the theoretical prediction that the micelle is able to accommodate fewer chains into the ensemble as the length of the soluble block is increased for a given insoluble block size.[18] Contrary to this, however, the experimentally found Q values for MA1 and MA4 are very similar, despite significant differences in N_A and in their dynamic behavior. For samples MA1 and MA3, the Q values calculated assuming good solvent conditions and $\varphi = 0.70$ agree reasonably well with experimental results; however, the R_h^s values are rather different. On the other hand, it is intriguing that the predictions for R_h^s and Q for our linear PS−PI diblock, sample DB, ($N_A = 2073$, $N_B = 250$) differ so much from the experimental results. A plausible explanation for these differences may come from the fact that SANS experiments are typically run at concentrations of 1 wt % (~6 mg/mL), which is 3 orders of magnitude greater than the concentrations used in this study. Therefore, the effects of concentration play an important role in the equilibrium structure of the spherical micelles as observed in previous studies[9,17] and in the current work. This suggests that these theoretical predictions may not work in the proximity of the micellar stability, i.e., at ultra low concentrations approaching the cmc.

It is also compelling to consider these micellar aggregates as a type of polymer brush, where the core/corona interface is the surface to which the branched PI chains are tethered.[39] Using a melt brush, Milner showed that the phase boundaries of asymmetric A_nB copolymer architectures depend substantially on the number of arms (n), due to the competition between bending of the A−B interface and stretching of the blocks away from the crowded interface.[40] Carignano and Szleifer also stated that the stretching of a solvated branched brush depended sensitively on the number of arms tethered at a single point set at the solid/fluid interface and also on the location of the branch point,[36] as alluded to earlier. In consideration of these works, as well as those of Pispas et al.,[16,17] it is likely that the organization of the branched PI−$(PI)_2$ blocks of the corona is different from the organization of chains in a corona made of linear PI chains. Moreover, and although the branch point is away from the core/corona interface, branching affects the size and aggregation of the whole ensemble, as observed from comparisons of samples DB, MA3, and MA4 presented herein.

Conclusions

Polystyrene−polyisoprene miktoarm block copolymers with a PS−PI−$(PI)_2$ architecture self-assemble into spherical micelles having PS cores and branched PI coronas when dissolved in *n*-hexane at concentrations of 30 and 3 μg/mL. These spherical micelles have hard-sphere diffusive behavior, as evidenced by the

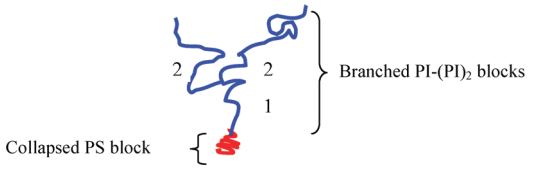

Figure 9. Representation of a PS−PI−$(PI)_2$ miktoarm copolymer. In the $R_{g,br}$ calculations only the branched PI−$(PI)_2$ blocks is taken into account.

steady value of the apparent diffusion coefficient obtained along the q-range studied, and as with micelles made from the linear block copolymers, aggregation number is strongly influenced by the degree of polymerization of the insoluble block. However, through comparisons with predictions from theory and properties of micelles formed from a diblock of similar total molecular weight and composition, it seems that while the micelles having branched coronal chains are more compact in hydrodynamic size, fewer chains can be accommodated in the ensemble. We attribute this behavior to the influence of branching in the corona, even though the branch point is not at the core/corona interface. Experiments at lower concentration (3 μg/mL) show similar patterns of behavior in micelle properties, with differences in the aggregation number to some extent. Comparison of the results with theoretical predictions based on the spherical micelles made of equivalent diblock copolymers show discrepancies in hydrodynamic size and aggregation number. These discrepancies may arise from the different internal arrangement of the branched blocks of the micellar corona or the use of experimentally found numerical prefactors found for linear self-assembled systems.

Acknowledgment. The donors of the Petroleum Research Fund, administered by the American Chemical Society, are gratefully acknowledged for partial support of this work. A portion of this work was conducted at the Center for Nanophase Materials Sciences (enabled through User Project 2008-297), which is sponsored at Oak Ridge National Laboratory by the Division of Scientific User Facilities, U.S. Department of Energy. Professor Paul Russo of Louisiana State University is acknowledged for fruitful discussions and Professor Jimmy W. Mays of the University of Tennessee, Knoxville is thanked for providing the materials used also in this study.

Appendix

The radius of gyration of single branched miktoarm PS−PI−$(PI)_2$ block copolymers, $R_{g,br}$, in n-hexane could not be determined by light scattering methods at concentrations below 3 μg/mL due the low $I(q)$ and incoherent scattering. However $R_{g,br}$ can be calculated from three different approaches based on chain statistics: (i) star homopolymer branching parameter, (ii) Yamakawa's branching parameter, and (iii) average arm calculations. Each approach is discussed and the equations required to determine $R_{g,br}$ are developed. The first two methods incorporate Flory's branching parameter, g, in the determination of geometric size for branched chains, where the $R_{g,br}$ of a branched PI homopolymer in n-hexane can be written as[41]

$$R_{g,br} = g^{1/2} b_{PI} N_{PI}^{\nu}, \quad \text{where } b_{PI} = 1.68\text{Å}, \ \nu = 0.57 \qquad \text{(A1)}$$

Here b_{PI} is the statistical segment size for PI. The values for b_{PI} and ν were calculated from intrinsic viscosity measurements.[41] Because n-hexane is a poor solvent for PS, it is assumed that the PS block is collapsed and, in the case of an isolated single chain, it does not contribute significantly to $R_{g,br}$ (see Figure 9). Therefore, the calculations treat the branched PI−$(PI)_2$ blocks only, and the results for each method are presented in Table 7.

Table 7. Radius of Gyration and Branching Parameter for PS−PI and PS−PI−$(PI)_2$ Miktoarm Block Copolymers in n-Hexane

			Star Homopolymer		Yamakawa		Avg. Arm	
sample ID	N_{PS}	N_{PI}	$R_{g,br}$ (nm)	g	$R_{g,br}$ (nm)	g	$R_{g,br}$ (nm)	g
DB	250	2073	13.1	1.00				
MA1	317	882	6.2	0.77	6.6	0.83	7.1	0.89
MA3	285	2294	10.6	0.77	11.0	0.80	12.3	0.89
MA4	317	2185	10.4	0.77	10.7	0.80	11.9	0.89

Knowing $R_{g,br}$ would be of use when interpreting the light scattering results, specifically whether the copolymers exist as isolated chains or as micellar aggregates in solution. Also, by determining g for each of the miktoarm samples, it is possible to properly "rescale" the values of N_A used in the comparisons of our experimental results with theoretical predictions for block copolymer micelles in dilute solution. As stated in this work, this rescaling helps to elucidate whether an "equivalent" diblock copolymer would show the same micellar properties as the miktoarms. The first two approaches allow the g parameter that properly describes the effects of branching in a polymer chain to be found, while the third approach uses a formula directly derived for PI homopolymer stars to determine their size.

Star Homopolymer Branching Parameter. The branching parameter, g, for any type of branched copolymer is defined as the ratio between the mean-squares of the radius of gyration of the branched polymer, $R_{g,br}$ and that of a linear polymer of the same molecular weight, $R_{g,l}$. Specifically, for monodisperse star homopolymers with f symmetrical arms, g can be written as[42]

$$g = \frac{\langle R_{g,br}{}^2 \rangle}{\langle R_{g,l}{}^2 \rangle} = \frac{3f-2}{f^2} \qquad \text{(A2)}$$

Equation A2 works well for Θ solvent conditions, but in the case of a good solvent, g is found to be ≈6% greater than the experimental value.[41] f is also called the functionality and it is defined as

$$f = M_{w,star}/M_{wa} \qquad \text{(A3)}$$

where $M_{w,star}$ is the total molecular weight of the star and M_{wa} is the molecular weight of a single arm (or branch). Considering the PI−$(PI)_2$ blocks of the miktoarms as a symmetric three-arm star, $g = 0.77$. This value is used in eq A1 to calculate $R_{g,br}$ for each of the samples studied based on their N_{PI}. The main drawback of this approach is that it does not take into account the asymmetry of the macromolecules. To address this shortcoming, a method proposed by Yamakawa is used to determine g. Yamakawa's method is based on the dividing the branched structure into subsegments between branching points.[43]

Yamakawa's Calculation of the g Branching Parameter. This method takes into account the size of each segment of the branched polymer; consequently, it can be used for nonsymmetrical arrangements. Yamakawa's g parameter is defined by[43]

$$g = \frac{1}{N^p}\left[\sum_{\lambda=1}^{p}(3NN_\lambda{}^2 - 2N_\lambda{}^3) + 6\sum_{(\lambda,\mu)} N_\lambda N_{\lambda\mu} N_\mu\right] \qquad \text{(A4)}$$

where N is the total number of segments or degree of polymerization of the whole branched polymer, N_λ the number of segments in the λth subsegment, p is the total number of subchains or branches. $N_{\lambda\mu}$ the number of segments in subchains that lie

between the λth and μth subchains. For the PI$-$(PI)$_2$ miktoarm stars, the second summation in eq A4 is zero because there are no segments between the subchains, which allows eq A4 for the PI$-$(PI)$_2$ branched homopolymer to be rewritten simply as

$$g = \frac{1}{N^3}[(3NN_1{}^2 - 2N_1{}^3) + 2(3NN_2{}^2 - 2N_2{}^3)] \qquad \text{(A5)}$$

Figure 9 identifies subchain 1 as the stem, while the two arms constitute the second subchains (which are labeled as 2 since both have the same N_{PI}). By using eq A5 it is possible to calculate g for the miktoarm stars and then use eq A1 to find $R_{g,br}$. These results are also given in Table 7.

Average Arm Calculations. The third approach is based on an average arm molecular weight, $M_{w,avg}$, which is calculated by dividing $M_{w,tot}$ by f. ($f = 3$ in the case of PI$-$(PI)$_2$.) $R_{g,br}$ is then calculated using the following formula derived from light scattering and intrinsic viscosity measurements of star PI homopolymers in cyclohexane, and it is applicable to stars of $f \geq 3$:[44]

$$R_{g,br} = 1.37f^{0.175}R_{g,avg} \qquad \text{(A6)}$$

Here the radius of gyration of the average arm, $R_{g,avg}$, is calculated by eq A1 using an average arm degree of polymerization, $N_{A,avg}$ and assuming $g = 1$. The $R_{g,br}$ results for the three approaches are summarized and the comparison of the g values obtained by each method is shown in Table 7.

The calculated $R_{g,br}$ values for the PI$-$(PI)$_2$ branched polymers show the expected trend, with sample MA1 having smallest value and sample MA3 having a slightly larger value of $R_{g,br}$ in comparison to MA4, which comes from the larger N_{PI} of the former. Because of its linear architecture, sample DB has a larger R_g in comparison to branched samples MA3 and MA4. (Again it is noted that samples DB, MA3, and MA4 have similar N_{PI}.) Concerning the g values obtained by each approach, the ones determined using the average arm approach are larger than those calculated using the two other approaches. In consideration of all the three methods, it is seen that $g \approx 0.8$, and therefore this value is used to "rescale" N_{PI} for use as parameter N_A in the calculations developed by Zhulina et al.[19] to compute Q and $R_h{}^s$ of spherical micelles based on a equivalent-sized linear diblock.

Supporting Information Available: Text describing the cumulant fittings, hard-sphere form factor for micellized PS$-$PI$-$(PI)$_2$ miktoarm block copolymers, and comparison of counting time in DLS experiments for sample MA3 and figures showing the fitting of the autocorrelation function for sample MA1, a plot of the mean decay rate, Γ_1, versus q^2, and dynamic light scattering experiments for sample MA3. This material is available free of charge via the Internet at http://pubs.acs.org.

References and Notes

(1) Hamley, I. W. *Block Copolymers in Solution: Fundamentals and Applications*; Wiley: West Sussex, U.K., 2005.
(2) Zana, R., Ed. *Dynamics of Surfactant Self-Assemblies Micelles, Microemulsions, Vesicles and Lyotropic Phases*; Taylor and Francis: Boca Raton, FL, 2005.
(3) Gohy, J.-F. *Adv. Polym. Sci.* **2005**, *190*, 65.
(4) Riess, G. *Prog. Polym. Sci.* **2003**, *28*, 1107.
(5) Ge, Z.; Liu, S. *Macromol. Rapid Commun.* **2009**, *30*, 1523.
(6) Bluhm, T.; Malthora, S. *Eur. Polym. J.* **1986**, *22*, 249.
(7) Bahadur, P.; Sastry, N.; Marti, S.; Riess, G. *Colloids Surf.* **1985**, *16*, 337.
(8) Price, C.; Canham, M.; Duggleby, M.; Naylor, T.; Rajab, N.; Stubbersfield, R. *Polymer* **1979**, *20*, 615.
(9) Adam, M.; Carton, J.-P.; Corona-Vallet, S.; Lairez, D. J. *Phys. II (Fr.)* **1996**, *6*, 1781.
(10) Bang, J.; Viswanathan, K.; Lodge, T. *J. Chem. Phys.* **2004**, *121*, 11489.
(11) Bang, J.; Jain, S.; Li, Z.; Lodge, T.; Pedersen, J.; Kesselman, E.; Talmon, Y. *Macromolecules* **2006**, *39*, 1199.
(12) Di Cola, E.; Lefebvre, C.; Deffieux, A.; Narayanan, T.; Borsali, R. *Soft Matter* **2009**, *5*, 1081.
(13) Farago, B.; Monkenbush, M.; Richter, D.; Huang, J.; Fetters, L.; Gast, A. *Phys. Rev. Lett.* **1993**, *71*, 1015.
(14) Minatti, E.; Viville, P.; Borsali, R.; Schappecher, M.; Deffieux, A.; Lazzaroni, R. *Macromolecules* **2003**, *36*, 4125.
(15) Lason, D.; Schappecher, M.; Deffieux, A.; Borsali, R. *Macromolecules* **2006**, *39*, 7107.
(16) Pispas, S.; Hadjichristidis, N.; Potemkin, I.; Khokhlov, A. *Macromoleclues* **2000**, *33*, 1741.
(17) Sotiriou, K.; Nannou, A.; Velis, G.; Pispas, S. *Macromolecules* **2002**, *35*, 4106.
(18) Halperin, A.; Alexander, S. *Macromolecules* **1989**, *22*, 2403.
(19) Zhulina, E.; Adam, M.; LaRue, I.; Sheiko, S.; Rubinstein, M. *Macromolecules* **2005**, *38*, 5330.
(20) LaRue, I.; Adam, M.; Zhulina, E.; Rubinstein, M.; Pisikalis, M.; Hadjichistidis, N.; Ivanov, D.; Gearba, R.; Anokhin, D.; Sheiko, S. *Macromolecules* **2008**, *41*, 6555.
(21) Hult, A.; Johansson, M.; Malmström, E. *Adv. Polym. Sci.* **1999**, *143*, 1.
(22) Chen, C.-C. *Langmuir* **2005**, *21*, 5605.
(23) Gestwicki, J.; Cairo, C.; Strong, L.; Oetjen, K.; Kiessling, L. *J. Am. Chem. Soc.* **2002**, *124*, 14922.
(24) Hinestrosa, J. P.; Alonzo, J.; Mays, J.; Kilbey, S. M. *Macromolecules* **2009**, *42*, 7913.
(25) Uhrig, D.; Mays, J. W. *J. Polym. Sci., Part A: Polym. Chem.* **2005**, *43*, 6179.
(26) *Polymer Handbook*, 4th ed.; Brandrup, J.; Immergut, E.; Grulke, E., Eds.; Wiley-Interscience: New York, 1999.
(27) Schärtl, W. *Light Scattering from Polymer Solutions and Nanoparticle Disperions*; Springer: Berlin, 2007.
(28) Provencher, S. *Comput. Phys. Commun.* **1982**, *27*, 229.
(29) Chu, B. *Laser Light Scattering: Basic Principles and Practice*; Dover: Mineola, 2007; p 248.
(30) Koppel, D. *J. Chem. Phys.* **1972**, *57*, 4814.
(31) Galinski, G.; Burchard, W. *Macromolecules* **1997**, *30*, 6966.
(32) Tuzar, Z.; Kratochvil, P. In *Light Scattering: Principles and Development*; Brown, W., Ed.; Oxford University Press: Oxford, U.K., 1996; p 327.
(33) Burchard, W. *Adv. Polym. Sci.* **1999**, *143*, 113.
(34) Semenov, A.; Vlassopoulos, D.; Fytas, G.; Vlachos, G.; Fleisher, G.; Roovers, J. *Langmuir* **1999**, *15*, 358.
(35) Daoud, M.; Cotton, J.-P. *J. Phys. (Fr.)* **1982**, *43*, 531.
(36) Carignano, M. A.; Szleifer, I. *Macromolecules* **1994**, *27*, 702.
(37) As pointed out by one of the manuscript reviewers.
(38) Lund, R.; Willner, L.; Linder, P.; Richter, D. *Macromolecules* **2009**, *42*, 2686.
(39) Halperin, A.; Tirell, M.; Lodge, T. P. *Adv. Polym. Sci.* **1992**, *100*, 31.
(40) Milner, S. *Macromolecules* **1994**, *27*, 2333.
(41) Tian, P. *Structure and Scaling of Polymer Brushes Formed by Branched Copolymers*. Ph.D. Dissertation, Clemson University: Clemson, SC, 2004.
(42) Mazur, J.; McCrakin, F. *Macromolecules* **1977**, *10*, 326.
(43) Yamakawa, H. *Modern Theory of Polymer Solutions*; Harper and Row: New York, 1971.
(44) Bauer, B.; Fetters, L.; Graessley, W.; Hadjichristidis, M.; Quack, G. *Macromolecules* **1989**, *22*, 2337.